LA-UR- 09-01435

Approved for public release;
distribution is unlimited.

Title:	A Spatial Light Modulator for Terahertz Beams
Author(s):	Hou-Tong Chen Antoinette J. Taylor
Intended for:	Nature Photonics

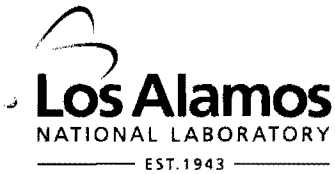

A Spatial Light Modulator for Terahertz Beams

Wai Lam Chan[1], Hou-Tong Chen[2], Antoinette J. Taylor[2], Igal Brener[3], Michael J. Cich[4], and Daniel M. Mittleman[1]*

[1]*Rice University, Department of Electrical and Computer Engineering, MS 366, Houston, Texas 77251-1892, USA*

[2]*Center for Integrated Nanotechologies, Los Alamos National Laboratory, PO Box 1663, MS K771, Los Alamos, New Mexico 87545, USA*

[3]*Center for Integrated Nanotechologies and Sandia National Laboratories, P. O. Box 5800, MS1082, Albuquerque, NM 87185*

[4]*Sandia National Laboratories, MS1085, Albuquerque, New Mexico 87185, USA*

* *E-mail: wailam@rice.edu*

Spatial light modulators that control the spatial transmission of a terahertz beam either electrically or optically, have been difficult to build due to the lack of suitable materials. Here we propose the use of active terahertz metamaterials[1-3] for the construction of a multi-pixel spatial modulator for terahertz beams. Our first-generation device consists of a 4x4 pixel array, where each pixel is an array of sub-wavelength-sized split-ring resonator

elements fabricated on a semiconductor substrate, and is independently controlled by applying an external voltage. Through terahertz transmission experiments, we show that the spatial modulator has a uniform modulation depth of around 40 percent across all pixels at the resonant frequency. Around this operating frequency, the crosstalk between pixels is negligible. This device can operate under small voltage levels, at room temperature, with low power consumption and reasonably high switching speed, and can therefore benefit future applications in terahertz imaging[4] and communications.[5,6]

Recent advances in terahertz technology and applications continuously drive the demand for novel terahertz devices. In the past decade, much research effort has been focused in the area of terahertz generation and detection,[7,8] while many functional devices for direct manipulation and processing of terahertz radiation are still lacking. One example is a spatial light modulator for terahertz beams. Spatial light modulators allow the optical or electrical control of the spatial transmission (or reflection) of an input light beam, and thus the ability to redirect or encode information in a wave front. Such devices are key components for many optical and optoelectronic systems, with applications in optical processing, optical interconnections, image display and real-time beam steering.[9,10] This technology, if extended to the terahertz region of the spectrum, can benefit exciting applications in terahertz imaging and communications. For instance, a recent single-pixel terahertz imaging system,[4] which is based on an advanced signal processing theory called compressed sensing,[11,12] requires a high-speed spatial modulator to encode random spatial patterns into the wave front of a terahertz beam.

The construction of a spatial terahertz modulator requires an array of small terahertz devices that can independently control the transmission of a terahertz beam at their respective array positions. Traditional technologies for spatial light modulators in the optical regime,[9,13]

which use liquid crystals, magneto-optic effects or deformable mirrors, do not operate efficiently in the terahertz regime because of the lack of materials with the desired terahertz response and/or the size mismatch between micro-machined devices and terahertz wavelengths. Terahertz modulators based on quantum-well structures either require cryogenic cooling[14] or have a poor modulation depth.[15] Other previous efforts in building terahertz modulators also yield modulation of only a few percent[16] or require high operation voltage.[17]

In this letter, we investigate the construction of a spatial terahertz modulator based on the use of active terahertz metamaterials.[1-3] This metamaterial device consists of a planar array of sub-wavelength-sized split-ring resonator (SRR) elements fabricated on a semiconductor (GaAs) substrate.[1] The control of the metamaterial resonance is realized by the depletion of substrate charge carriers upon voltage bias which in turn changes the effective capacitance of all of the individual SRR elements within a pixel, thereby modifying the terahertz transmission. The device enables a modulation depth >50% under a relatively small bias voltage (16 volts) at room temperature. Moreover, fast modulation, in the megahertz range, is achievable.[2] The design of such metamaterial devices is flexible because the resonant frequency can be tuned by changing the geometry and dimensions of the SRR elements.[18] The use of frequency-agile metamaterials even allows dynamic tunability with external optical control.[19] Compared to existing terahertz modulators,[14-17] the metamaterial-based electrical terahertz modulator is very promising for the construction of a high-speed spatial modulator.

Our first demonstration of a THz spatial modulator is a 4×4 pixel array, where each pixel is a 4×4 mm^2 array of metamaterial SRRs, as shown in Fig. 1. The dimensions of the SRR elements are designed such that the device has a resonant transmission at 0.36 THz upon application of a voltage. Each pixel is independently controlled by an external voltage across a

1×1 mm^2 Schottky electric pad and the ohmic contact. This device has low power dissipation, drawing only a few milliamperes of current even when all the pixels are dc-biased at 14 volts.

We characterize our spatial modulator in a transmission geometry using a terahertz time-domain spectroscopy system with fibre-coupled photoconductive antennae for both terahertz generation and detection. The linearly-polarized terahertz beam is collimated and directed towards the modulator, as shown in Fig. 2, with the polarization of the terahertz electric field aligned along the direction across the split-gap of the SRRs on the modulator. In these experiments, we raster-scan the terahertz receiver across the beam, after it has passed through the modulator. The substrate lens of the receiver antenna is covered by a metal mask with a 1 mm aperture to improve the spatial resolution of the measurement. At each receiver position, we measure the terahertz waveform using an optical chopper in the terahertz beam and a lock-in amplifier to filter the signal from the photoconductive antenna. Fig. 3a shows the typical transmission spectra for one of the 16 pixels in the "on" and "off" configurations, i.e., under a dc bias voltage of 0 or 14 volts, respectively. For all 16 pixels, we observe a modulation depth between 35% and 50% at the designed resonant frequency of 0.36 THz. Shown in Fig. 3b is the transmission image of the 4-by-4 modulator array at 0.36 THz, with two pixels turned off (biased) and the rest turned on (zero bias). Images at other frequencies look similar, but with less contrast because of the lower modulation depth at these frequencies. To study the uniformity of the modulation depth within individual pixels, we select a few pixels in the array and observe the standard deviation of the modulation depth within these pixels to be around 10%. Our experimental results show a rather uniform modulation depth both within individual pixels and across all pixels in our modulator.

One of the important issues in any multi-pixel modulator is the amount of crosstalk

among the pixels. To investigate this potential concern, we remove the optical chopper from the terahertz beam and instead modulate only certain pixel elements directly by applying a square-wave ac voltage bias, alternating between 0 and 14 V. Using a lock-in amplifier referenced to this square wave, we can then detect very small amount of crosstalk, if any, in the un-modulated pixels. The terahertz modulation signals are detected at every receiver position of the raster-scan to produce the transmission image in Fig. 4a. Signals with the largest amplitudes are concentrated at the two modulated pixels, with only a small amount of crosstalk in the surrounding pixels. To take into account the effect of system noise, we perform another raster-scan with all pixels unbiased and unmodulated (while the lock-in amplifier is still referenced to the square wave voltage frequency). From the first dataset, for each frequency, we calculate $\frac{N+C}{S}$, the ratio of the signal power at the surrounding un-modulated pixels (due to both crosstalk, C, and noise, N) to the signal power at the modulated pixel, S (dashed red curve in Fig. 4b). We then calculate $\frac{N}{S}$, the ratio of the noise power from the second dataset to S from the first dataset (solid blue curve). The difference between the two ratios gives the crosstalk level, independent of the system noise. This procedure is necessary because the crosstalk is so small as to be nearly indistinguishable from the noise.

As shown in Fig. 4b, the crosstalk level (solid black curve) is larger (–15 dB) at lower frequencies due to diffraction effects, but drops to around –30 dB near 0.33 THz. Above this frequency, quantifying the amount of crosstalk becomes challenging, because the noise-to-signal ratio increases significantly, making the crosstalk indistinguishable from system noise. As a result, we regard this measurement to be an upper limit on the crosstalk at the device operating frequency.

To provide an illustration of the switching capability of our spatial modulator, we modulate certain pixel elements dynamically for two distinct configurations. Shown in the insets of Fig. 5 are two double-slit configurations. The white pixel elements are driven by a 3 kHz square wave varying between 0 and 14 volts. This frequency is also used as the reference for the lock-in amplifier. The array elements shown in grey are unbiased. We use a lens to focus the transmitted terahertz wave front, and the terahertz detector (with a 1 mm aperture) is scanned along a line in the focal plane of the lens, across a 64 mm interval. Fig. 5 shows the measured differential fringe patterns (solid blue curves) at 0.36 THz for the two double-slit configurations. These have the same slit sizes (b = 4 mm) but different slit separations (a = 8 mm and 12 mm respectively for the upper and lower panels in Fig. 5). As expected, the fringes appear at distances, multiples of $\lambda f/a$, away from the central fringe. Here, λ is the observation wavelength, f is the focal length of the focusing lens and a is the slit separation. Analytical calculations of the double-slit diffraction pattern, assuming a plane wave illumination, best fit our measured data with a = 9.8 mm and 13.8 mm respectively for the two configurations, and b = 5 mm (see red curves in Fig. 5). When using metal slits of the same dimensions as those of the slits formed by the modulator in a direct observation of the diffraction fringes, we observe similar values for these fit parameters. This indicates that the differences between the fit parameters and the actual geometrical dimensions of the double slit are a result of the fact that the illuminating terahertz beam is not an ideal plane wave. To our knowledge, this is the first demonstration of fast dynamical modulation of a terahertz wave front.

To conclude, we have implemented the first electrical spatial terahertz modulator based on a metamaterial structure with electric split-ring resonator elements fabricated on a semiconductor substrate. Our first-generation design, a 4-by-4 pixel array, demonstrates a high

modulation depth at the resonant frequency, uniformly within individual pixels and across all pixels, and the amount of crosstalk among pixels is negligible. We demonstrate the kHz-rate operation of this spatial modulator by measuring a double slit configuration to generate interference patterns. Our spatial modulator features favourable operating conditions (small voltage levels at room temperature) and low power consumption. Slight modifications to our metamaterial design can also achieve spatial phase modulation[3] (instead of amplitude) or dynamic tunability of the resonant frequency,[19] rendering numerous possible applications of the device in future terahertz imaging and communication systems.

Acknowledgements

W.L.C. and D.M.M. acknowledge partial support from the National Science Foundation and from the Air Force Office of Scientific Research through the CONTACT program. H.T.C and A.J.T. acknowledge support from the Los Alamos National Laboratory LDRD Program. This work was performed, in part, at the Center for Integrated Nanotechnologies, a US Department of Energy, Office of Basic Energy Sciences Nanoscale Science Research Center operated jointly by Los Alamos and Sandia National Laboratories. Sandia is a multiprogram laboratory operated by Sandia Corporation, a Lockheed Martin Company, for the United States Department of Energy's National Nuclear Security Administration under Contract DE-AC04-94AL85000.

Competing financial interests The authors declare that they have no competing financial interests.

Figure captions

Figure 1 Design of electrically driven terahertz metamaterial spatial modulator. The spatial modulator (not drawn to scale) is a 4×4 pixel array, where each pixel is a 4×4 mm^2, 2500-element array of metamaterial SRRs fabricated on epitaxial *n*-doped GaAs grown on an semi-insulating GaAs substrate. Within each pixel, the SRR elements have 200 nm gold thickness, 4 μm line width, 2 μm split gap spacing, 66 μm outer dimension and 76 μm period. Each pixel is independently controlled by an external voltage across a 1×1 mm^2 Schottky electric pad and the ohmic contact.

Figure 2 Transmission setup for characterization of the terahertz spatial modulator. The linearly-polarized terahertz beam is collimated and directed towards the modulator, with the polarization of the terahertz electric field aligned along the direction across the split-gap of the SRRs on the modulator. The terahertz receiver detects the waveform transmitted across the spatial modulator at each pixel position, while various spatial patterns are applied on the modulator through external voltage controls. A metal square aperture (1×1 mm^2) placed in front of the receiver antenna enables measuring of a small area of the transmitted terahertz wavefront.

Figure 3 Electrically controllable terahertz transmission spectra through the spatial modulator. a, Terahertz amplitude transmission spectra for one of the 16 pixels of the spatial terahertz modulator without voltage bias (red) and with 14V bias (blue). A large modulation depth is observed at 0.36 THz, the designed resonant frequency. **b,** A transmission image of the 4-by-4 array at 0.36 THz, with two pixels turned off (biased), and the rest turned on (zero bias).

Figure 4 Terahertz transmission crosstalk among pixels of the spatial modulator. a, A transmission image of the 4-by-4 array of the spatial terahertz modulator at 0.36 THz, with two pixels under a square voltage bias alternating between 0 and 14 volts, and the rest unbiased. A terahertz modulation (differential) signal is measured at each pixel. **b,** Noise-to-signal power ratio (blue) and noise-plus-crosstalk-to-signal power ratio (red) across frequency, obtained respectively when all pixels are unbiased and when one pixel is biased with a square voltage. The difference between these two curves yields the crosstalk level (black), i.e., the crosstalk-to-signal power ratio, across frequency. Above 0.33 THz (in the shaded area), the level of crosstalk is nearly equivalent to the noise, and is therefore unmeasurable. The lowest measured crosstalk, −30 dB, is therefore an upper limit on the crosstalk at the design frequency of the device.

Figure 5 Double-slit experiments with the terahertz spatial modulator. Measured (solid blue curves) fringe patterns produced by the transmission of the terahertz beam through the spatial terahertz modulator in two double-slit configurations. The insets show the "on" and "off" configurations of the 16 pixels, with zero bias on the grey pixels, and the white pixels modulated with a 3-kHz square signal alternating between 0 and 14V. With a lock-in amplifier referenced to this square wave, the measured signal is the difference between two diffraction patterns, one in which all the pixels are biased at zero volts, and the other in which the white pixels are biased and the grey pixels are not. The dashed red curves show the predicted values computed using simple plane wave diffraction theory.

References

1. Chen, H.-T. et al. Active terahertz metamaterial devices. *Nature* 444, 597-600 (2006).

2. Chen, H.-T. et al. Hybrid metamaterials enable fast electrical modulation of freely propagating terahertz waves. *App. Phys. Lett.* 93, 091117 (2008).

3. Chen, H.-T. et al. A metamaterial solid-state terahertz phase modulator. *Nat. Photonics* advance online publication, 22 February 2009 (DOI 10.1038/nphoton.2009.3).

4. Chan, W. L. et al. A single-pixel terahertz imaging system based on compressed sensing. *App. Phys. Lett.* 93, 121105 (2008).

5. Kleine-Ostmann, T., Pierz, K., Hein, G., Dawson, P. & Koch, M. Audio signal transmission over THz communication channel using semiconductor modulator. *Elec. Lett.* 40, 124-126 (2004).

6. Jastrow, C. et al. 300 GHz transmission system. *Elec. Lett.* 44, 213-214 (2008).

7. Ferguson, B. & Zhang, X.-C. Materials for terahertz science and technology. *Nat. Materials* 1, 26-33 (2002).

8. Siegel, P. H. THz technology. *IEEE Trans. Microwave Theory Tech.* 50, 910-928 (2002).

9. Efron, U. *Spatial Light Modulator Technology: Materials, Devices and Applications* (CRC Press, U.S.A., 1995).

10. Xun, X., Chang, X. & Cohn, R. System for demonstrating arbitrary multi-spot beam steering from spatial light modulators. *Opt. Express* 12, 260-268 (2004).

11. Candes, E., Romberg, J. & Tao, T. Robust Uncertainty Principles: Exact Signal reconstruction from highly incomplete frequency information. *IEEE Trans. on Information Theory* 52, 489-509 (2006).

12. Donoho, D. Compressed Sensing. *IEEE Trans. on Information Theory* 52, 1289-1306 (2006).

13. Goodman, J. W. *Introduction to Fourier Optics* (Roberts and Company Publishers, U.S.A., 2004).

14. Kersting, R., Strasser, G. & Unterrainer, K. Terahertz phase modulator. *Elec. Lett.* 36, 1156-1158 (2000).

15. Libon, I. H. et al. An optically controllable terahertz filter. *App. Phys. Lett.* 76, 2821-2823 (2000).

16. Kleine-Ostmann, T., Dawson, P., Pierz, K., Hein, G. & Koch, M. Room-temperature operation of an electrically driven terahertz modulator. *App. Phys. Lett.* 84, 3555-3557 (2004).

17. Kuzel, P., Kaldec, F., Petzelt, J., Schubert, J. & Panaitov, G. Highly tunable $SrTiO_3/DyScO_3$ heterostructures for applications in the terahertz range. *App. Phys. Lett.* 91, 232911 (2007).

18. Azad, A. K., Taylor, A. J., Smirnova, E. & O'Hara, J. F. Characterization and analysis of terahertz metamaterials based on rectangular split-ring resonators. *App. Phys. Lett.* 92, 011119 (2008).

19. Chen, H.-T. et al. Experimental demonstration of frequency-agile terahertz metamaterials. *Nat. Photonics* 2, 295-298 (2008).

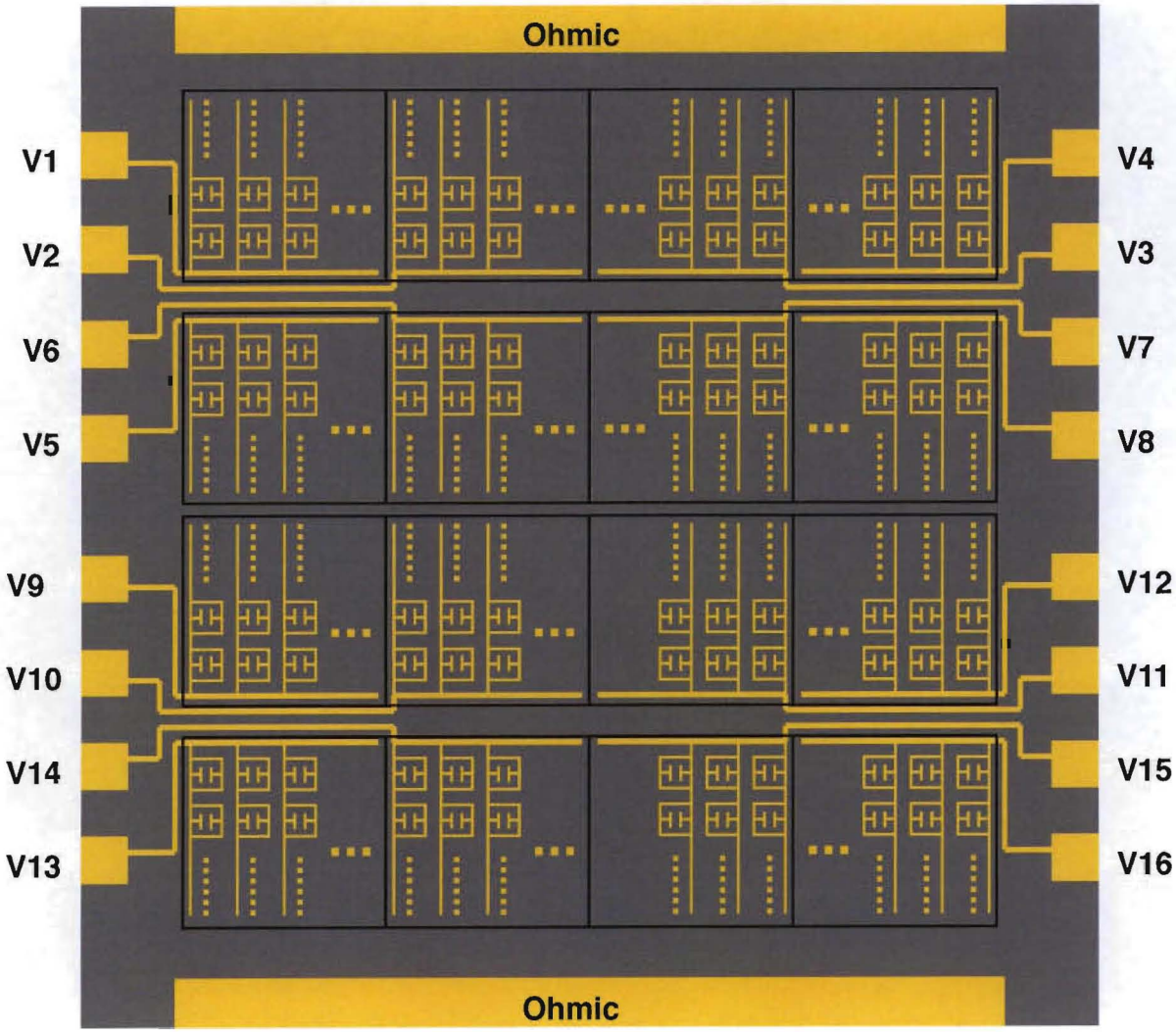
Ohmic
V1
V2
V6
V5
V9
V10
V14
V13
V4
V3
V7
V8
V12
V11
V15
V16
Ohmic

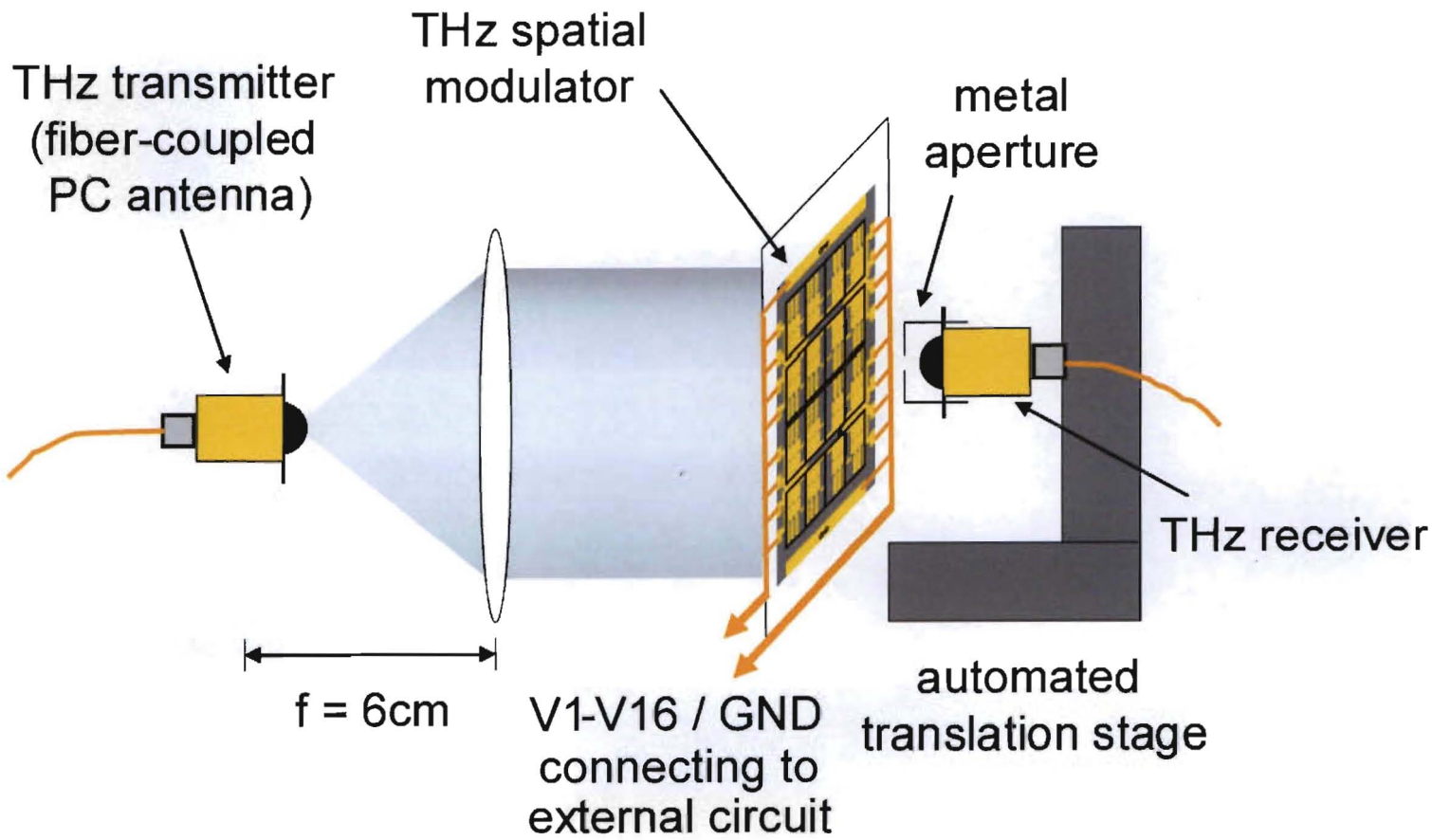
THz transmitter
(fiber-coupled
PC antenna)
THz spatial
modulator
metal
aperture
THz receiver
f = 6cm
V1-V16 / GND
connecting to
external circuit
automated
translation stage

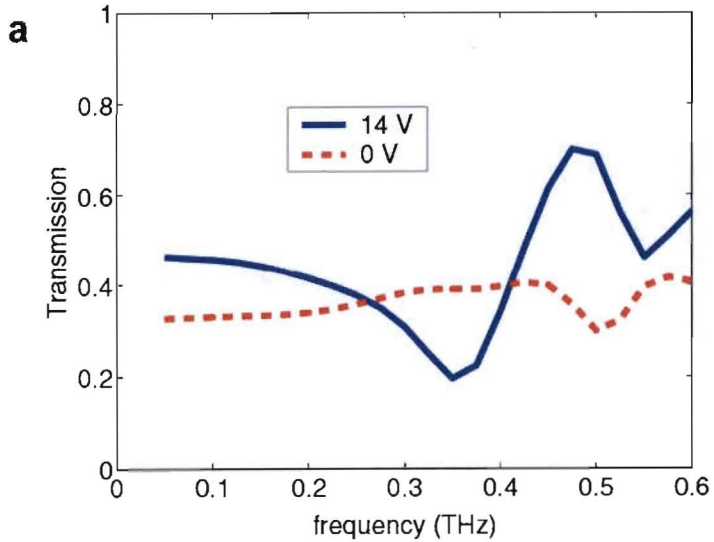
a
1
0.8
0.6
0.4
0.2
0
Transmission
14 V
0 V
0
0.1
0.2
0.3
0.4
0.5
0.6
frequency (THz)

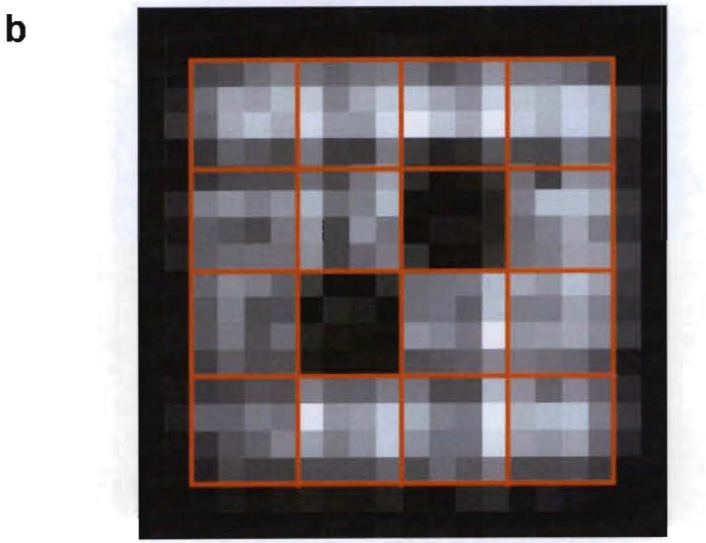
b

a

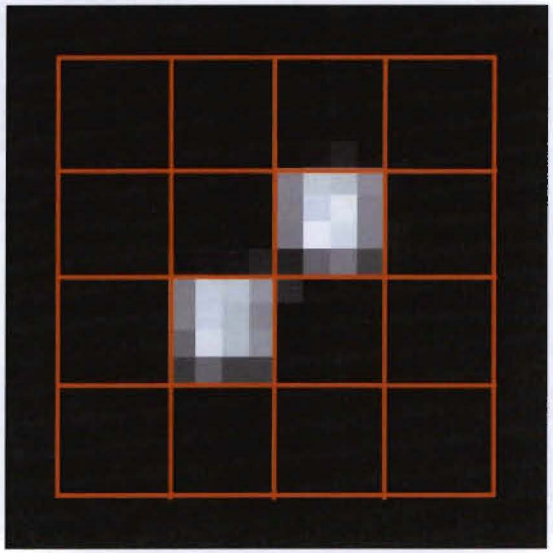

b

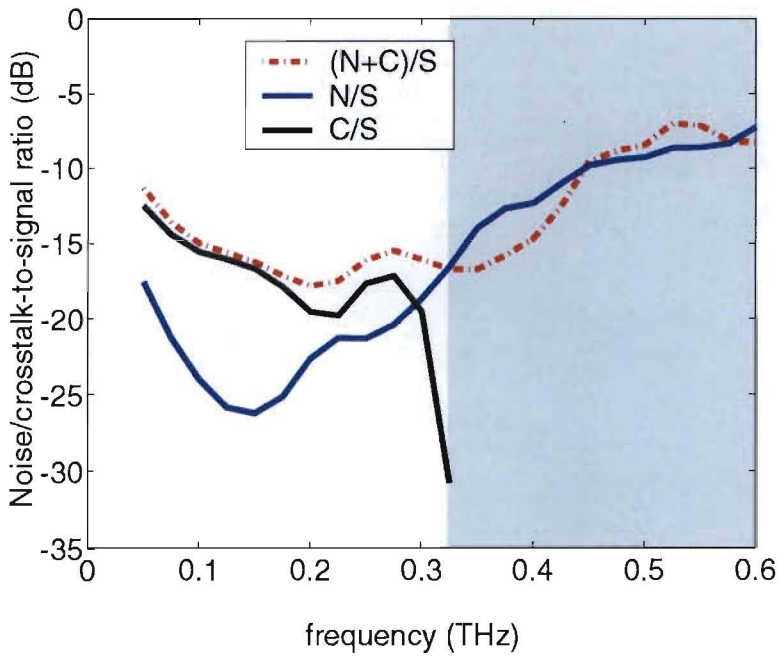
(N+C)/S
N/S
C/S
Noise/crosstalk-to-signal ratio (dB)
0
-5
-10
-15
-20
-25
-30
-35
0
0.1
0.2
0.3
0.4
0.5
0.6
frequency (THz)

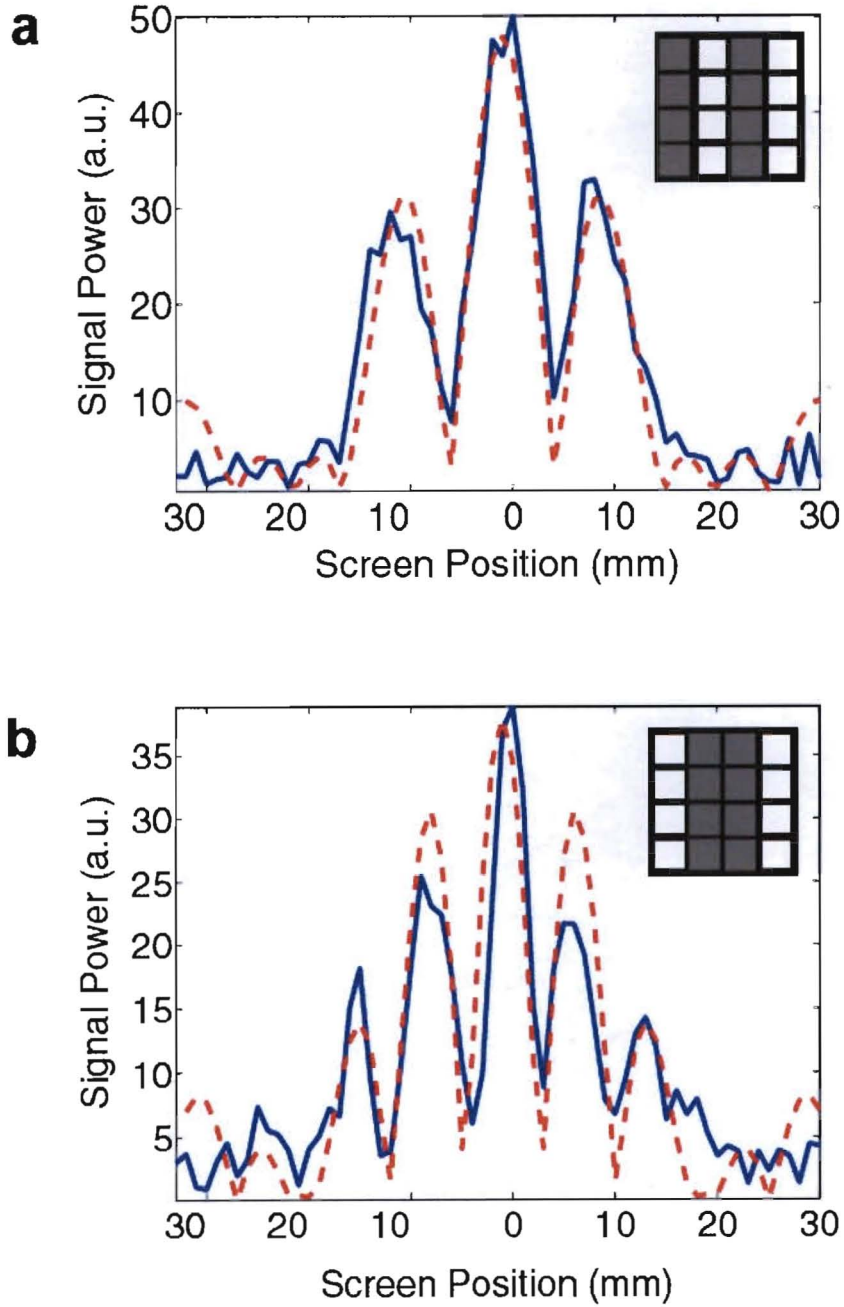
a
Signal Power (a.u.)
50
40
30
20
10
30
20
10
0
10
20
30
Screen Position (mm)
b
Signal Power (a.u.)
35
30
25
20
15
10
5
30
20
10
0
10
20
30
Screen Position (mm)